Neural Comput & Applic (2015) 26:237–250
DOI 10.1007/s00521-014-1721-y

ORIGINAL ARTICLE

ANN and multiple regression method-based modelling of cutting forces in orthogonal machining of AISI 316L stainless steel

F. Kara · K. Aslantas · A. Çiçek

Received: 7 September 2013 / Accepted: 14 September 2014 / Published online: 27 September 2014

Abstract In this study, predictive modelling was performed for the cutting forces generated during the orthogonal turning of AISI 316L stainless steel. An artificial neural network (ANN) and a multiple regression analysis were utilised. The input parameters of the ANN model were the cutting speed, feed rate and coating type. In the model, tungsten carbide cutting tools, uncoated and with two different coatings (TiCN + Al_2O_3 + TiN and Al_2O_3), were used. The ANN predictions closest to the experimental cutting forces were obtained for the main cutting force (F_c) and the feed force (F_f) by 3-7-1 and 3-6-1 network architectures with a single hidden layer, respectively. While the SCG learning algorithm provided the optimal results for F_c, the optimal results for F_f were provided by the LM learning algorithm. A very good performance of the neural network, in terms of agreement with the experimental data, was achieved. With the developed model, the cutting forces could be precisely predicted depending on the cutting speed, feed rate and coating type. The prediction results showed that the ANN was superior to the multiple regression method in terms of prediction capability.

Keywords Cutting forces · Orthogonal machining · Artificial neural network · Coating materials

F. Kara (✉)
Department of Manufacturing Engineering, Faculty of Technology, University of Düzce, Konuralp Campus, 81620 Düzce, Turkey
e-mail: fuatkara@duzce.edu.tr

K. Aslantas
Department of Mechanical Engineering, Faculty of Technology, University of Afyon Kocatepe, A.N.S. Campus, 03200 Afyonkarahisar, Turkey

A. Çiçek
Department of Mechanical Engineering, Faculty of Engineering and Natural Sciences, Yıldırım Beyazıt University, Ankara, Turkey

1 Introduction

Due to their high resistance to corrosion and oxidation, austenitic stainless steels have been commonly used in many industrial areas including those of aircraft, nuclear, defence, food processing and particularly in that of medicine [1–4]. However, the machining of these steels is very difficult because of their high ductility, work hardening rate and low thermal conductivity [5]. The proper selection of cutting parameters in the machining of these steels plays a significant role in ensuring the quality of the product, reducing the machining costs and increasing productivity [6]. In addition, poor selection of the cutting parameters causes a decrease in the surface quality as well as rapid cutting tool wear [7–10]. Measurement of the cutting forces is of great importance in the determination of the optimum cutting parameters because the cutting forces are one of the most significant factors affecting tool life [11–15].

In scientific studies carried out to determine the optimum cutting parameters, expensive experimental setups and long test durations are needed. For this reason, different analyses, optimisation and modelling techniques have been developed, including finite element analysis, the multiple regression method, the Taguchi method, fuzzy logic, genetic algorithms and artificial neural networks (ANN) [16–20]. In recent years, many ANN-based scientific studies have been performed due to the good prediction capability of this technique [21–23]. Owing to its

memorisation and analytical skills, an ANN resembles a simple imitation of the human brain. Solving systems for which the solutions are not analytically possible or for which a mathematical model cannot be completely structured has become easier through ANNs, which arose from computer programs affected by natural neural systems [24, 25]. The ANN method is used in the machining area as well. In the chip-removal process, a wide range of factors, including environmental conditions, rigidity and surface roughness, as well as cutting parameters, should be taken into account. The ANN method is mostly used for the prediction of surface roughness and cutting forces. In their studies, Hao et al. [26] used ANNs to develop a model for the prediction of the cutting forces in a self-propelled rotating tool during the turning process. In the constructed ANN architecture, while the cutting speed, feed rate, depth of cut and inclination angle were used as inputs, the main cutting force, feed force and radial force were outputs of the network. They created a new hybrid model by combining the ANN model with the genetic algorithm. Through the new hybrid model, cutting forces could be obtained that were very close to the experimental data. Suksawat [27] presented an ANN application that predicted the main cutting force and the classified chip form. The cutting speed, feed rate and depth of cut were used as inputs to a network for predicting the cutting force and classified chip form occurring during the turning of nylon material with HSS tools. As a result of the study, the convergence values for the predictions of the classified chip form and the cutting force were calculated with 86.67 and 91.13 % accuracy. Ozkan et al. [28] developed an ANN model for the prediction of the cutting forces and temperatures generated in the turning process under different cutting conditions. By means of the developed model, the cutting forces and temperature values could be predicted precisely. In another study, a back propagation neural network model has been developed for the prediction of surface roughness in turning operation by Pal and Chakraborty [18]. The convergence of the mean square error both in training and testing came out very well. The performance of the trained neural network has been tested with experimental data and found to be in good agreement. Yilmaz et al. [29] performed a study about predicting the surface roughness by means of neural network approach method on machining of a cast polyamide material. The network has two inputs called spindle speed and feed rate for this study. Gradient descent method was applied to optimise the weight parameters of neuron connections. According to the predicted results, the ANN model developed for predicting the surface roughness values in milling gave correct and acceptable results.

For the present study, an ANN model was developed for the prediction of the main cutting force and feed force occurring during orthogonal cutting. In the input layer of the ANN architectures, the coating type (C_t), feed rate (f) and cutting speed (V) are included. In addition, multiple regression analysis was performed for the same input and output parameters. The cutting force values calculated using the formulas obtained from both an ANN and a multiple regression analysis were compared with the experimentally measured cutting force values.

2 Materials and methods

2.1 Experimental process

Orthogonal turning tests using AISI 316L austenitic stainless steel bars (see Table 1) as the workpiece material were carried out on a Johnford T35 CNC lathe with 10-kW spindle power and a maximum spindle speed of 6,500 rpm. The experimental setup for orthogonal cutting is shown in Fig. 1. The bars, 60 mm in diameter and 240 mm in cutting length, were turned with two different coated and uncoated cemented carbide cutting inserts. The workpiece and cutting tools used in the orthogonal cutting tests are shown in Fig. 2. A Kistler piezoelectric dynamometer model 9257B with a load amplifier connected to a computer was used for the acquisition of the cutting force (F_c) and feed force (F_f). The orthogonal cutting tests were carried out at feed rates of 0.05, 0.1 and 0.2 mm/rev, cutting speeds of 75, 100, 150, 200 and 250 m/min and a constant depth of cut of 2 mm (Table 2). General properties of cutting inserts produced by Iscar used in the machining of AISI 316L are given in Table 3. The inserts had a $-6°$ rake angle, 5° clearance angle and 0.8 mm nose radius. In cutting experiments, tool holder was used the tool holder code of PTGNL 2525M16 and approaching angle of 90°. The mechanical and thermal properties of the coating materials are given in Table 4 [30].

2.2 Artificial neural networks

An ANN is a data processing and modelling technique that arose in pursuit of mathematical modelling of the learning process which was inspired by the human brain. The ANN concept arose as the idea of imitating the brain's working principles on digital computers. The studies on this subject started in 1942 with the mathematical modelling of neurons, the biological units that constitute the brain, and the application of this model to computer systems; afterwards, it was utilised in many fields in parallel with the development of computer systems. ANNs have the ability to associate the input data, defined depending on single or multiple parameters, regarding a system with that system's outputs, defined depending on single or multiple

Table 1 Chemical characteristics (wt%) of AISI 316L material

C	Mn	Si	P	S	Ni	Cr	Mo	Fe
0.017	1.50	0.520	0.029	0.0010	11.20	16.75	2.15	67.833

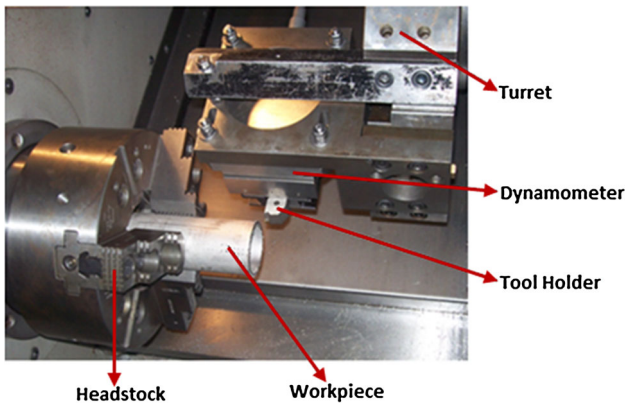

Fig. 1 Experimental setup for orthogonal cutting

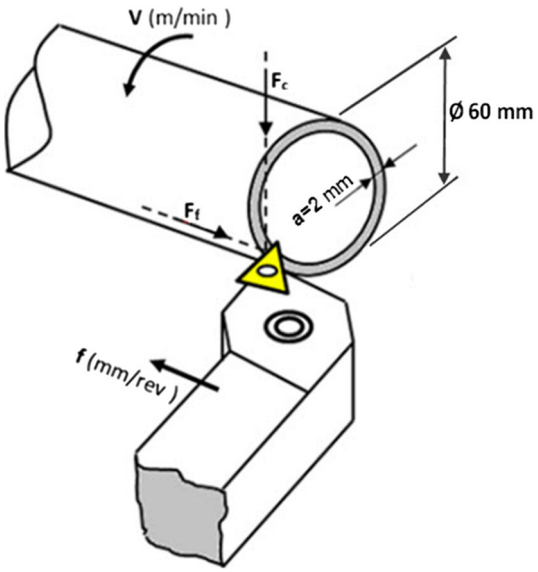

Fig. 2 Workpiece material used in orthogonal cutting process

Table 2 Test parameters

Workpiece material	AISI 316L
Coating type	Uncoated, TiCN + Al_2O_3 + TiN, Al_2O_3
Cutting speed (V, m/min)	75, 100, 150, 200, 250
Feed rate (f, mm/rev)	0.05, 0.1, 0.2, 0.3
Depth of cut (a, mm)	2

Table 3 Cutting inserts used in the experimental study

ISO grade	Insert code	Coating method	Coating type	Total coating thickness (μm)
M10–M25 K10–K20	IC20	–	Uncoated	–
K05–K20	IC4028	CVD	TiCN + Al_2O_3 + TiN	(2 + 2+1) ~5
P05–P15 K05–K20	IC428	CVD	Al_2O_3	~5

parameters [31]. The biggest advantage of ANNs is that they are able to learn and to use different learning algorithms [32]. In ANNs, the data coming from the external world go to the input layer. These are the data that we want the network to learn. The way that data are given to the network varies with respect to the data set. The summation function (Σ) is a function that calculates the net input coming to a cell, and the net input is generally a sum of multiplications of the inputs (x) with the relevant weights (w), calculated with the formula in Eq. (1).

$$\mathrm{NET}_i = \sum_{j=1}^{n} w_{ij} x_j + w_{bi} \tag{1}$$

where NET_i is the weighted summation of the input values, i and j are processing elements, n is the number of processing elements in the previous layer, w_{ij} is the weight of the connections between the i and j processing elements, x_j is the output of the j processing element and w_{bi} is the weight of the biases between layers.

At the next stage, the output of the summation function is sent to the transfer (activation) function. This function transforms the received value into a real output through an algorithm. As regards the transfer function used, the output values are usually normalised between −1 and 1 [33] or between 0 and 1 [34]. The transfer functions used in ANNs are generally nonlinear functions. Using nonlinear transfer functions allows ANNs to be applied to very different complex problems. The common transfer functions in ANNs are linear, step/signum, threshold, logistic sigmoid, hyperbolic tangent sigmoid functions, etc. In the ANN model developed in this study, the logistic sigmoid transfer function was used and its formula is given in Eq. (2).

Table 4 The mechanical and thermal properties of coating and uncoated materials [30]

Material	TiN	TiCN	Al_2O_3	WC (uncoated)
Coating thickness (μm)	1.5–3	4–8	3–5	–
Hardness (HV)	2,300	3,000	2,000	
Thermal expansion coefficient ($\times 10^{-6}$) (K^{-1})	9.4	8	8.4	5
Modulus of elasticity (GPa)	600	448	415	650
Poisson ratio	0.25	0.23	0.22	0.25
Density (kg/m^3)	4,650	4,180	3,780	11,900
Heat capacity (N/mm^2 °C)	3	2.5	3.42	15
Thermal conductivity (W/m °C)	20 (40 °C)	26 (25 °C)	33 (50 °C)	30 (30 °C)
	21 (100 °C)	27 (100 °C)	28 (90 °C)	32 (100 °C)
	22 (300 °C)	28 (300 °C)	19 (300 °C)	34 (300 °C)
	23.5 (500 °C)	30.5 (500 °C)	13 (500 °C)	37 (500 °C)
	26 (1,000 °C)	33.5 (1,000 °C)	7 (1,000 °C)	44 (1,000 °C)
	27 (1,300 °C)	35 (1,300 °C)	7 (1,300 °C)	47.5 (1,300 °C)

$$f(\mathrm{NET}_i) = \frac{1}{1 + e^{-\mathrm{NET}_i}} \tag{2}$$

where f(NET) is the logistic sigmoid transfer function.

The significant advantages of ANNs are their learning ability and their use of different learning algorithms. In order to obtain the output values closest to the experimental values, the best learning algorithm and the optimal number of neurons in the hidden layer should be determined. Different types of learning algorithms used in the network training process include gradient descent back propagation (GD), quasi-Newton back propagation (BFGS), Levenberg–Marquardt back propagation (LM), scaled conjugate gradient back propagation (SCG), resilient back propagation (RP), conjugate gradient back propagation with Polak–Ribiére updates (CGP) and Bayesian regulation back propagation (BR). The most important factor that determines its success in practice, after the construction of ANN architecture, is the learning algorithm. In this study, the LM, SCG, BFGS, RP and CGP learning algorithms were used for network training. In addition, the number of hidden layers and neurons in each hidden layer were determined. Of the 60 experimental data obtained as a result of an experimental study, 48 data were randomly selected as training data, while 12 data were selected as testing data. An investigation of previous studies in the literature found the data numbers used in this study to be adequate for ANN modelling (Kohli and Dixit [35]—31 data; Pal and Chakraborty [36]—27 data; Cus and Zuperl [37]—30 data; Al-Ahmari [38]—28 data; Davim et al. [39]—30 data; Karnik et al. [40]—36 data; Chavoshi and Tajdari [41]—18 data; Korkut et al. [17]—50 data; Asiltürk et al. [42]—27 data). The input and output values were normalised between 0.1 and 0.9. The normalisation values of the network are given in Table 5. Finally, the iteration number was entered and the training process was started. The data obtained from the ANN training were compared with the cutting force values obtained experimentally from the cutting tests. For comparison, the root mean square error (RMSE), R^2 (coefficient of determination) and mean error percentage (MEP) values were used. These values are calculated with the formulas given in Eqs. (3–5).

$$\mathrm{RMSE} = \left(\left(\frac{1}{p}\right)\sum_j \left|t_j - o_j\right|^2\right)^{1/2} \tag{3}$$

$$R^2 = 1 - \left(\frac{\sum_j \left(t_j - o_j\right)^2}{\sum_j \left(o_j\right)^2}\right) \tag{4}$$

$$\mathrm{MEP}\,(\%) = \frac{\sum_j \left(\left(t_j - o_j\right)/t_j\right) \times 100}{p} \tag{5}$$

where t is the target value, p is the number of patterns and o is the output value. The cutting parameters and coating types used for turning AISI 316L austenitic stainless steel under orthogonal conditions and the experimental cutting force values obtained as a result of the cutting tests are given in Table 6. As shown in Table 6, the digits for the coating type to be entered into the multiple regression analysis and the ANNs were determined as: uncoated = 1, TiCN + Al_2O_3 + TiN-coated = 2 and Al_2O_3-coated = 3.

The ANN architectures for the prediction of the cutting forces are shown in Fig. 3. In the ANN architecture constructed for the main cutting force, three neurons (coating type, cutting speed and feed rate) were included in the input layer, seven neurons were included in its hidden layer and one neuron was included in the output layer. In addition, in the ANN architecture constructed for the feed force, three neurons were included in the input layer, six neurons were included in its hidden layer and one neuron was included in the output layer.

Table 5 Normalization values of inputs and outputs

No	C_t	V (m/min)	f (mm/rev)	F_c (N)	F_f (N)	No	C_t	V (m/min)	f (mm/rev)	F_c (N)	F_f (N)
1	0.25	0.25	0.15	0.28540	0.407097	31	0.5	0.5	0.6	0.544324	0.49871
2	0.25	0.25	0.3	0.40050	0.508387	32	0.5	0.5	0.9	0.762162	0.581935
3	0.25	0.25	0.6	0.63513	0.694839	33	0.5	0.66666	0.15	0.191351	0.234194
4	0.25	0.25	0.9	0.89351	0.885806	34	0.5	0.66666	0.3	0.304324	0.325806
5	0.25	0.33333	0.15	0.24702	0.338065	35	0.5	0.66666	0.6	0.504324	0.433548
6	0.25	0.33333	0.3	0.35567	0.423871	36	0.5	0.66666	0.9	0.718378	0.51871
7	0.25	0.33333	0.6	0.59621	0.590968	37	0.5	0.83333	0.15	0.195135	0.247742
8	0.25	0.33333	0.9	0.83027	0.712258	38	0.5	0.83333	0.3	0.303784	0.325161
9	0.25	0.5	0.15	0.193514	0.237419	39	0.5	0.83333	0.6	0.521081	0.421935
10	0.25	0.5	0.3	0.323784	0.328387	40	0.5	0.83333	0.9	0.684324	0.490323
11	0.25	0.5	0.6	0.53027	0.425806	41	0.75	0.25	0.15	0.204324	0.247097
12	0.25	0.5	0.9	0.736757	0.510323	42	0.75	0.25	0.3	0.346486	0.368387
13	0.25	0.66666	0.15	0.187568	0.216129	43	0.75	0.25	0.6	0.601622	0.581935
14	0.25	0.66666	0.3	0.315135	0.287742	44	0.75	0.25	0.9	0.847027	0.727097
15	0.25	0.66666	0.6	0.5	0.371613	45	0.75	0.33333	0.15	0.19027	0.232258
16	0.25	0.66666	0.9	0.702703	0.427097	46	0.75	0.33333	0.3	0.341081	0.36
17	0.25	0.83333	0.15	0.191351	0.209032	47	0.75	0.33333	0.6	0.570811	0.518065
18	0.25	0.83333	0.3	0.307568	0.263226	48	0.75	0.33333	0.9	0.764865	0.576129
19	0.25	0.83333	0.6	0.500541	0.330968	49	0.75	0.5	0.15	0.177838	0.194194
20	0.25	0.83333	0.9	0.671351	0.38	50	0.75	0.5	0.3	0.30973	0.319355
21	0.5	0.25	0.15	0.223784	0.270968	51	0.75	0.5	0.6	0.54	0.445161
22	0.5	0.25	0.3	0.351892	0.408387	52	0.75	0.5	0.9	0.720541	0.51871
23	0.5	0.25	0.6	0.605946	0.607742	53	0.75	0.66666	0.15	0.176757	0.212258
24	0.5	0.25	0.9	0.856757	0.774194	54	0.75	0.66666	0.3	0.296216	0.285806
25	0.5	0.33333	0.15	0.224865	0.283226	55	0.75	0.66666	0.6	0.481081	0.378065
26	0.5	0.33333	0.3	0.335135	0.37871	56	0.75	0.66666	0.9	0.684865	0.457419
27	0.5	0.33333	0.6	0.578378	0.563871	57	0.75	0.83333	0.15	0.183784	0.207097
28	0.5	0.33333	0.9	0.811351	0.669032	58	0.75	0.83333	0.3	0.298919	0.278065
29	0.5	0.5	0.15	0.182162	0.209677	59	0.75	0.83333	0.6	0.494595	0.36129
30	0.5	0.5	0.3	0.317297	0.346452	60	0.75	0.83333	0.9	0.667027	0.429677

3 Results and discussion

3.1 Experimental evaluation of the main cutting force

As a result of the experimental studies, the change in the main cutting force obtained under the same conditions for each tool used is given in Fig. 4. As can be seen clearly from the diagrams, increases in the main cutting force depend on an increased feed rate. Since the increase in the feed rate leads to an increase in the chip cross section, the pressure affecting the cutting tool will also increase. Consequently, the force required for cutting will increase. In addition, another common point in the main cutting force results obtained for each of the three cutting tools is that the cutting force rates obtained for low cutting speeds are high. In a sense, as the cutting force decreases, it becomes harder to break chips off the workpiece. As the cutting speed increases, the cutting temperature in the first deformation zone increases and thermal softening occurs in the cutting zone. This in turn leads to a decrease in the cutting force. Similar results were found in the literature [43, 44].

When Fig. 4 is examined, it can be observed that the increase in the feed rate leads to a linear increase in the main cutting force. Additionally, it can be seen that as the cutting speed increases, the main cutting force decreases proportionally. It is possible to say that the cutting force obtained for the uncoated cutting tool is higher when compared with that of the TiCN + Al_2O_3 + TiN-coated and the Al_2O_3-coated cutting tools. This condition can be seen clearly, especially when the maximum cutting forces obtained for 75 m/min cutting speed and 0.3 mm/rev feed rate are compared with each other. The reason for this is the low thermal conductivity coefficient of the coating materials [30].

Table 6 Experimental cutting force values

Cutting speed (m/min)	Feed rate (mm/rev)	Uncoated (1)		$TiN + Al_2O_3 + TiCN$ (2)		Al_2O_3 (3)	
		F_c (N)	F_f (N)	F_c (N)	F_f (N)	F_c (N)	F_f (N)
75	0.05	528	631	414	420	3,788	383
75	0.1	741	788	651	633	641	571
75	0.2	1,175	1,077	1,121	942	1,113	902
75	0.3	1,653	1,373	1,585	1,200	1,567	1,127
100	0.05	457	524	416	439	352	360
100	0.1	658	657	620	587	631	558
100	0.2	1,103	916	1,070	874	1,056	803
100	0.3	1,536	1,104	1,501	1,037	1,415	893
150	0.05	358	368	337	325	329	301
150	0.1	599	509	587	537	573	495
150	0.2	981	660	1,007	773	999	690
150	0.3	1,363	791	1,410	902	1,333	804
200	0.05	347	335	354	363	327	329
200	0.1	583	446	563	505	548	443
200	0.2	925	576	933	672	890	586
200	0.3	1,300	662	1,329	804	1,267	709
250	0.05	354	324	361	384	340	321
250	0.1	569	408	562	504	553	431
250	0.2	926	513	964	654	915	560
250	0.3	1,242	589	1,266	760	1,234	666

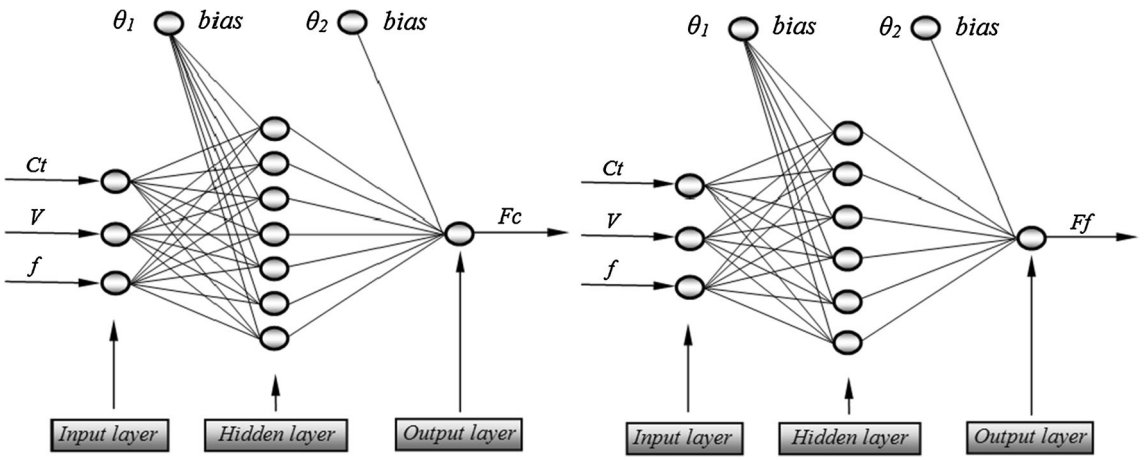

Fig. 3 Single hidden layer ANN architectures created for cutting forces

In particular, the thermal conductivity of the Al_2O_3 coating decreases with increased temperature [45]. Thus, the spread of the heat occurring within the tool is delayed [46]. Most of the occurring heat is focused on the cutting zone. This in turn leads to a decrease in the cutting force because the increased cutting temperature decreases the friction coefficient in the tool–chip interface [47] and causes thermal softening in the workpiece.

3.2 Experimental evaluation of the feed force

The variations in feed forces obtained from the experimental studies conducted are given in Fig. 5. Depending on the increased feed rate, the feed forces in the three tools also increase. In addition, depending on the increased cutting speed, the feed forces decrease [44, 48]. The fact stands out that the feed forces obtained with an uncoated

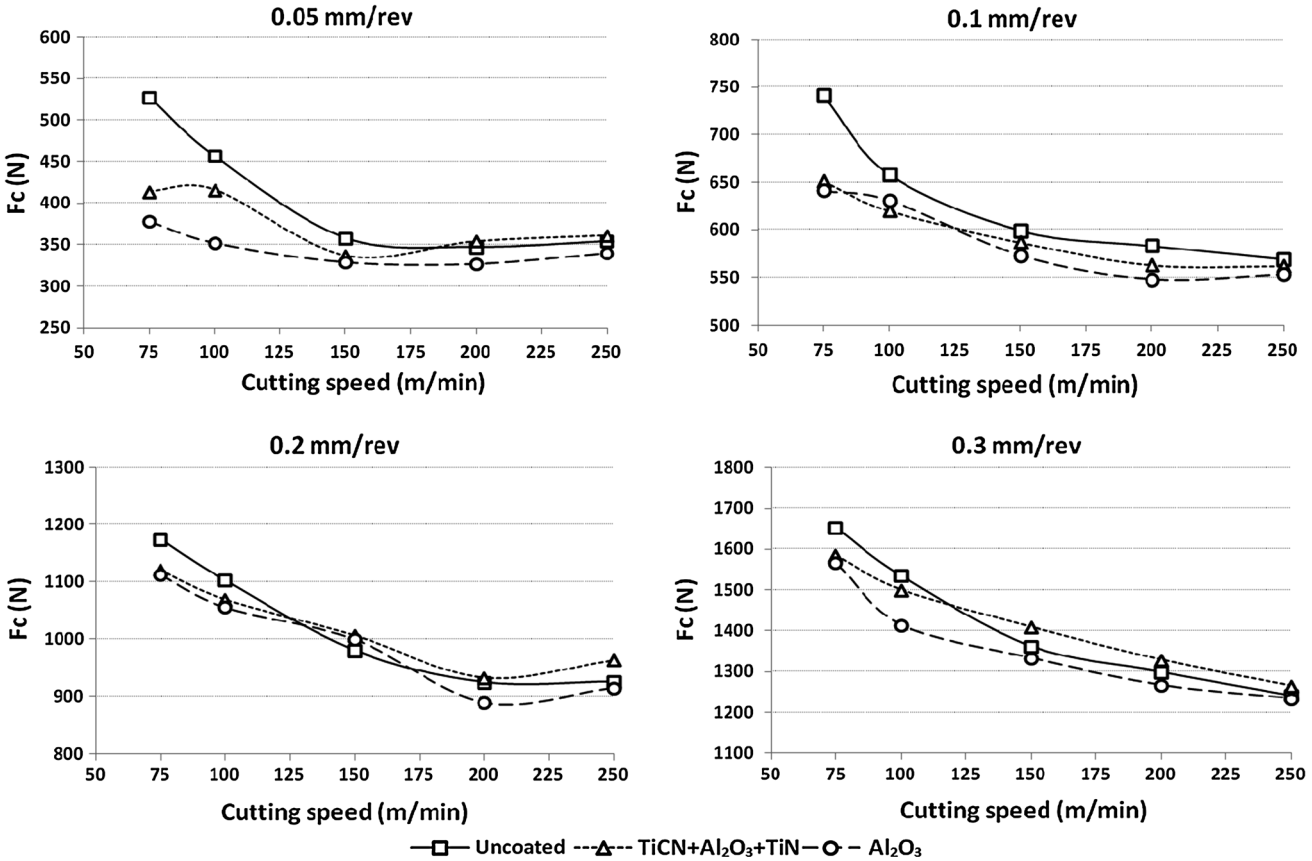

Fig. 4 The variations in main cutting force depending on the coating type and cutting speed

cutting tool at cutting speeds of $V = 75$ and 100 m/min are higher than the results obtained with the other two cutting tools. However, it is possible to say that the feed forces obtained at other cutting speeds are closer to each other. According to Fig. 5, the feed forces obtained with uncoated tools are higher than the feed forces obtained with the Al_2O_3-coated cutting tool. In addition, the F_f obtained with the TiCN + Al_2O_3 + TiN-coated cutting tool for $V \geq 150$ m/min and $f \geq 0.2$ mm/rev is higher than that obtained with the uncoated tool. However, it can be said that there are no significant differences between TiCN + Al_2O_3 + TiN-coated and uncoated tools for $V \geq 150$ m/min and $f \leq 0.1$ mm/rev. This was attributed to low thermal conductivity coefficient of the coating material. Low thermal conductivity of the coated cutting tools exhibits better performance compared with uncoated cutting tools [30, 49, 50].

When both main cutting and feed forces were evaluated together, the cutting of AISI 316L stainless steel material at 150 m/min and higher cutting speeds may be more advantageous in terms of tool life because it is clear that at cutting speeds lower than 150 m/min in all three types of tools, the main cutting and feed forces are very high. On the other hand, when the cutting tools are evaluated within themselves, it is possible to say that the forces obtained for the Al_2O_3-coated cutting tool are lower. The thermal conductivity of the Al_2O_3 coating decreases with increased temperature [45]. Therefore, the Al_2O_3-coated cutting tool exhibits better performance compared with TiCN + Al_2O_3 + TiN-coated and uncoated tools [30, 49].

3.3 Prediction of cutting forces using multiple regression analysis

The variance analyses performed for the main cutting force and feed force are given in Table 7. As is apparent from the table, the effects of all the cutting parameters ($Pr = 0.0067$, $Pr < .0001$, $Pr < .0001$) on the main cutting force are statistically significant. Here, $Pr < 0.05$ value indicates statistically significant of parameters. This situation shows that the coating type, cutting speed and feed rate have a significant effect on the main cutting force in the orthogonal cutting process. Nevertheless, when the F statistical values are considered, it is possible to say that the feed rate has a greater effect on the main cutting force when compared with the coating type and cutting speed.

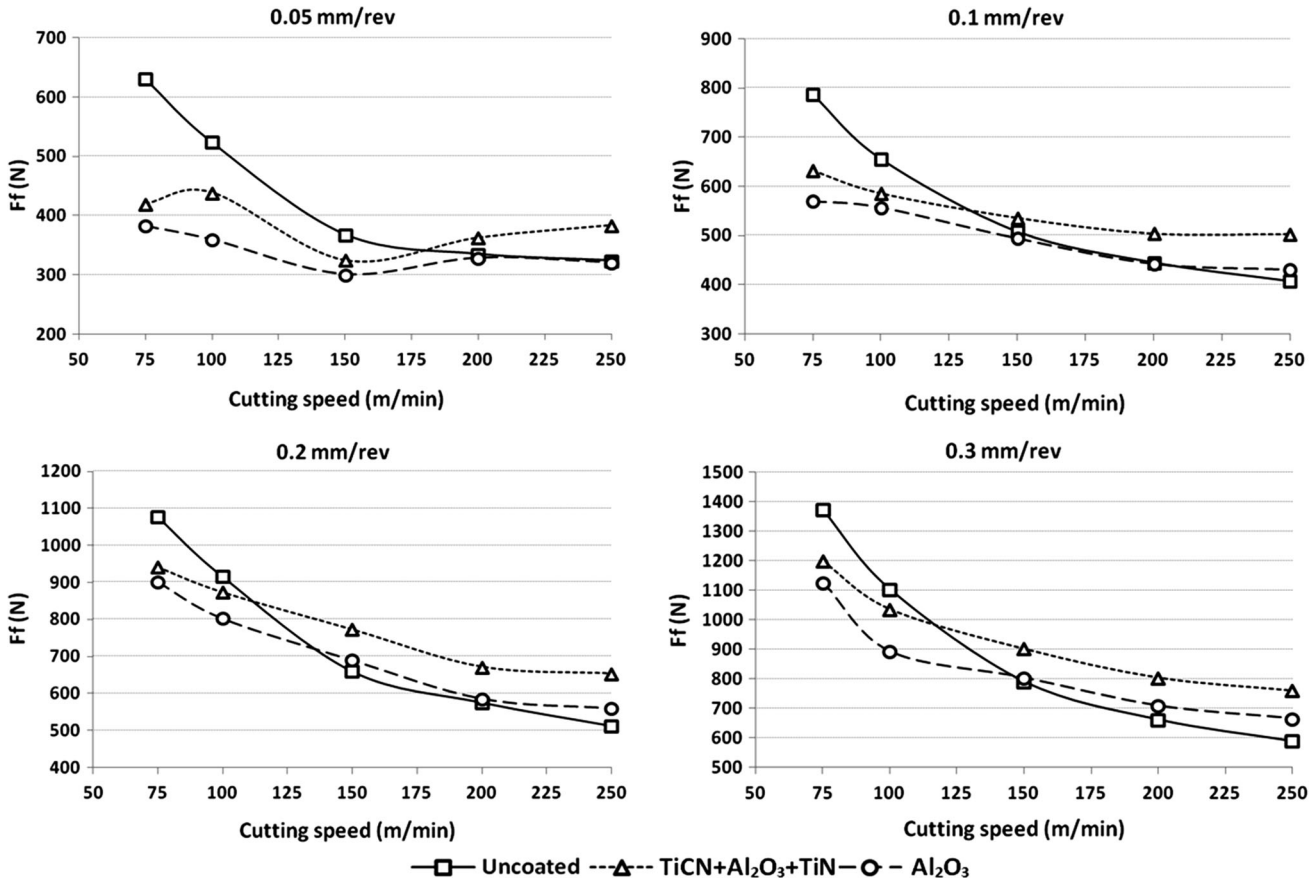

Fig. 5 The variations in feed force depending on the coating type and cutting speed

Table 7 Variance analysis for main cutting force and feed force

Source	Degrees of freedom (*df*)	Sum of square (SS)	Mean square	*F* value	Pr > *F*
F_c					
Model	3	9,490,655.9	3,163,552	1,144.281	<.0001
Coating type	1	21,949.2	21,949.2	7.9392	0.0067
Cutting speed	1	287,463.8	287,463.8	103.9779	<.0001
Feed rate	1	9,181,242.8	9,181,242.8	3,320.927	<.0001
Error	56	154,821.1	2,765	<.0001	
Total	59	9,645,477			
F_f					
Model	3	3,049,486.2	1,016,495	104.8405	<.0001
Coating type	1	53,728.9	53,728.9	5.5416	0.0221
Cutting speed	1	764,316.9	764,316.9	78.8310	<.0001
Feed rate	1	2,231,440.4	2,231,440.4	230.1489	<.0001
Error	56	542,955.7	9,696	<.0001	
Total	59	3,592,441.9			

When the significance values in the variance analysis conducted for the feed force are considered, it can be seen that the cutting parameters (coating type $Pr = 0.0221$, cutting speed $Pr < .0001$, feed rate $Pr < .0001$) are effective on the feed force. The *F* statistical values of the feed rate, coating type and cutting speed parameters are

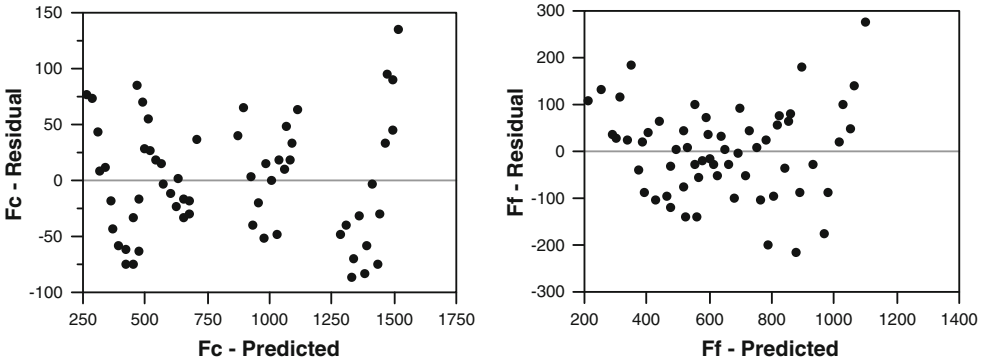

Fig. 6 Comparison of cutting force values predicted by using regression analysis with residual cutting force values

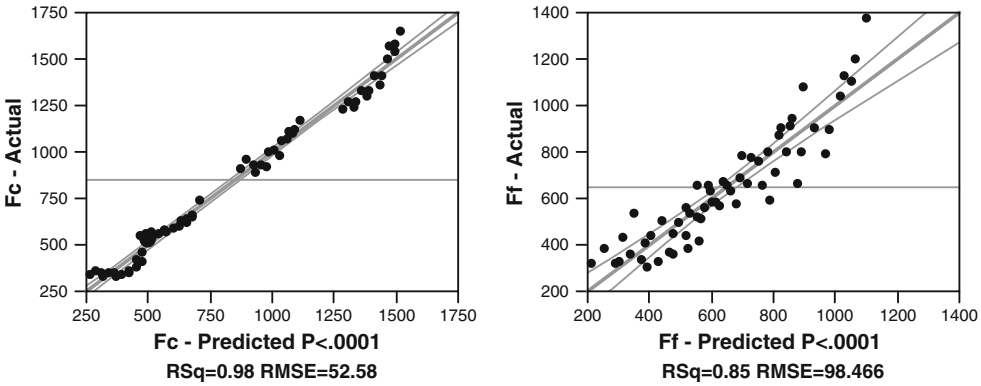

Fig. 7 Comparison of experimental results with cutting force values predicted by using regression analysis

230.1489, 5.5416 and 78.8310, respectively. These values show that the feed rate that has the highest F statistical value has a greater effect on the feed force when compared with the coating type and cutting speed. The statistical results obtained through multiple regression analysis for the main cutting force and feed force are given in Figs. 6 and 7. The mathematical statements established with multiple regression analysis for the main cutting force and feed force are given in Eqs. (6) and (7).

$$F_c = ((400.851) - ((23.425) \cdot C_t) - ((1.080) \cdot V) + ((4,074.169) \cdot f)) \quad (6)$$

$$F_f = ((664.757) - ((36.650) \cdot C_t) - ((1.762) \cdot V) + ((2,008.542) \cdot f)) \quad (7)$$

The variations in the predicted cutting forces depending on the experimental results are given in Fig. 6. While the maximum deviation values vary between 150 and −100 for the main cutting force, the maximum deviation values for the feed force are between 300 and −250. This is also an indication that the coefficient of determination of the feed force is lower. The variations in the cutting force values predicted with multiple regression analysis, as per the experimental cutting force values, are given in Fig. 7. The predicted main cutting force values are very close to the experimental cutting force values. It was determined that the best convergence value was 99.96 % and the worst convergence value was 77.65 %, whereas for the feed force, it was found that the best convergence value was 99.69 % and the worst convergence value was 65.42 %. Also, the coefficients of determination for the main cutting force and feed force resulting from the regression analysis were 0.98 and 0.85, respectively.

3.4 Prediction of cutting forces using artificial neural networks

In the training of the ANN model developed for obtaining the cutting forces, five different learning algorithms, namely LM, SCG, BFGS, RP and CGP, were used to determine the optimum learning algorithm. Also, by using a range of network architectures, from three neurons to ten neurons, the optimum network architecture was determined. As a result of trials, while the optimum results for the main cutting force were obtained by the network architecture with seven neurons in its hidden layer and by the SCG learning algorithm, the optimum results for the feed force were obtained by the LM learning algorithm and

Table 8 Statistical data for the main cutting forces using five different algorithms

Learning algorithm	Number of neurons	Training data			Testing data		
		RMSE	R^2	MEP	RMSE	R^2	MEP
SCG	3	0.015306	0.999106	3.589901	0.013884	0.999180	2.706918
SCG	4	0.009467	0.999658	1.480786	0.013993	0.999174	3.514036
SCG	5	0.008724	0.999710	1.700779	0.013431	0.999235	3.065112
SCG	6	0.007488	0.999786	1.276862	0.011329	0.999457	2.435329
SCG	*7*	*0.006674*	*0.999830*	*1.396251*	*0.007364*	*0.999771*	*1.447662*
SCG	8	0.004564	0.999921	0.875680	0.017976	0.998671	3.475144
SCG	9	0.004564	0.999921	1.116395	0.023382	0.997645	3.542660
SCG	10	0.004564	0.999921	1.033962	0.027418	0.996897	5.188471
LM	3	0.011260	0.999517	2.093985	0.012519	0.999329	2.415376
LM	4	0.008837	0.999702	1.358820	0.019276	0.998442	4.275722
LM	5	0.009429	0.999661	1.719516	0.011035	0.999483	2.163731
LM	6	0.007663	0.999776	1.395324	0.017538	0.998712	3.221716
LM	7	0.004564	0.999921	0.871082	0.015970	0.998932	3.879227
LM	8	0.004482	0.999923	1.145517	0.017449	0.998681	3.100300
LM	9	0.004554	0.999921	0.916429	0.016680	0.998806	3.838557
LM	10	0.004442	0.999925	1.036134	0.022302	0.997828	3.064588
BFGS	3	0.015227	0.999116	3.562690	0.013814	0.999189	2.693845
BFGS	4	0.008232	0.999742	1.591950	0.020150	0.998310	4.491831
BFGS	5	0.009142	0.999682	1.669994	0.011785	0.999413	2.347815
BFGS	6	0.008439	0.999729	1.712332	0.013133	0.999270	2.746763
BFGS	7	0.008170	0.999746	1.647688	0.011950	0.999393	2.259466
BFGS	8	0.007176	0.999804	1.293539	0.009509	0.999616	2.157031
BFGS	9	0.006180	0.999854	1.274929	0.017918	0.998624	3.384065
BFGS	10	0.004562	0.999921	0.863788	0.022545	0.997893	4.021354
RP	3	0.015415	0.999093	3.576337	0.012891	0.999290	2.531734
RP	4	0.012331	0.999420	2.470526	0.013562	0.999215	3.154455
RP	5	0.010335	0.999593	2.032983	0.010626	0.999523	2.269514
RP	6	0.009022	0.999690	1.638328	0.013198	0.999256	2.692624
RP	7	0.008194	0.999744	1.868142	0.011574	0.999438	2.358093
RP	8	0.007928	0.999760	1.473474	0.009242	0.999638	1.999521
RP	9	0.006937	0.999817	1.541089	0.009218	0.999634	2.132322
RP	10	0.006167	0.999855	1.067891	0.015161	0.999053	3.038948
CGP	3	0.026177	0.997373	6.087994	0.022788	0.997897	4.164616
CGP	4	0.011111	0.999529	2.575415	0.011671	0.999416	2.217321
CGP	5	0.016594	0.998947	3.475182	0.016420	0.998873	3.934075
CGP	6	0.009914	0.999625	2.088262	0.011475	0.999437	2.604078
CGP	7	0.011513	0.999495	2.467319	0.014016	0.999177	2.992922
CGP	8	0.010350	0.999592	2.180787	0.011702	0.999422	2.750823
CGP	9	0.011659	0.999482	2.478784	0.013824	0.999186	2.430141
CGP	10	0.005819	0.999871	1.220104	0.013854	0.999193	2.687012

Italic values show the optimum results for the main cutting force obtained by the network architecture with seven neurons in its hidden layer and by the SCG learning algorithm

by the network architecture with six neurons in its hidden layer. The network architectures developed for the main cutting force and the statistical results obtained for the learning algorithms are given in Table 8.

The matching of the experimental and ANN values for testing and training sets of the main cutting forces is shown in Figs. 8 and 9, respectively. Additionally, the matching of the experimental and ANN values for testing and

training sets of feed forces is shown in Figs. 10 and 11, respectively. They consist of the results of 60 tests that were performed using uncoated, TiCN + Al_2O_3 + TiN- and Al_2O_3-coated cutting tools. The most significant point here is that the prediction values are very close to the experimental values. As shown in Figs. 8, 9, 10 and 11, the predictive ability of the network for F_c and F_f was found to be satisfactory. This means that the selection of three input parameters as influencing factors for predictions of main cutting forces and feed forces provided satisfactory results. Among the algorithms developed for the prediction of cutting forces, the statistical values of the learning algorithm and network architecture that provided the best results are given in Table 9.

Having selected the most suitable network architectures and learning algorithms, the mathematical statements established using the ANN model developed for the prediction of cutting force values are given in Eqs. (8) and (9).

$$F_c = \left(\frac{1}{1 + e^{-(5.1916 \times F1 + 0.5208 \times F2 - 0.4575 \times F3 - 7.0998 \times F4 + 2.3128 \times F5 + 1.0023 \times F6 - 1.9508 \times F7 + 1.9509)}} \right) \times 1{,}850 \quad (8)$$

$$F_f = \left(\frac{1}{1 + e^{-(0.5889 \times F1 + 0.4594 \times F2 + 0.7798 \times F3 - 5.9822 \times F4 - 132.2598 \times F5 - 0.6642 \times F6 + 132.7910)}} \right) \times 1{,}550 \quad (9)$$

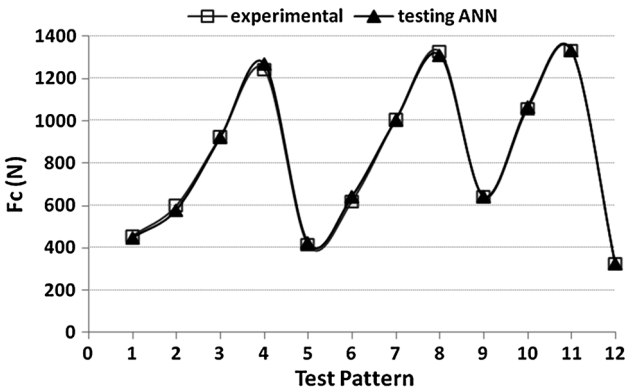

Fig. 8 Matching of the experimental and ANN values for testing sets of main cutting forces

where F_i ($i = 1, 2, 3, \ldots, 6$ or 7) can be calculated according to Eq. (10).

$$F_i = \frac{1}{1 + e^{-E_i}} \quad (10)$$

where E_i is the weighted sum of the input and is calculated by the equation given in Tables 10 and 11.

The weight values show the effects of the parameters existing in the input layer on the cutting force values. The weight values obtained for the main cutting force and feed force are given in Tables 10 and 11. As seen in Table 10, the most effective parameter, which affects the main cutting force positively and negatively, is the feed rate.

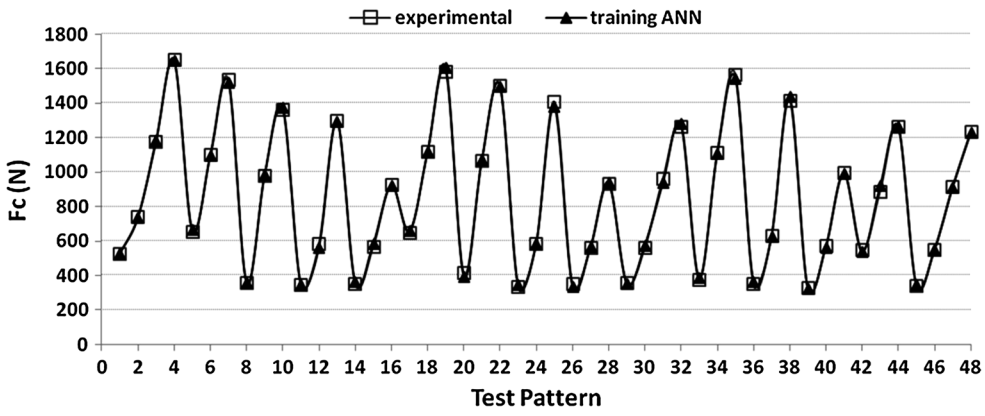

Fig. 9 Matching of the experimental and ANN values for training sets of main cutting forces

It can be seen clearly from the weight values in Table 11 that, while the most effective input affecting the feed force positively is the feed rate, the most negatively effective input is the cutting speed. The maximum error values for the cutting force values obtained as a result of the ANN predictions are given in Table 12. The deviation values in Table 10 provide the evidence that the ANN model developed is a valid model.

4 Conclusions

In this study, the multiple regression method and an ANN were used for the prediction of the cutting forces that occur during the orthogonal turning of AISI 316L austenitic stainless steel. Several cutting experiments were conducted during the experimental stage of the study by taking different cutting parameters and coating types into consideration. The findings of the study are as follows:

1. When the experimental and ANOVA results were examined, the dominant factor affecting both the main cutting force and the feed force was the feed rate. The feed rate was followed by the cutting speed and coating type, respectively.
2. The best results in the prediction of the main cutting force were obtained by the network architecture with seven neurons in its hidden layer and the SCG learning algorithm, whereas the best results for the feed force prediction were obtained with the network architecture having six neurons in its hidden layer and the LM learning algorithm. Because coefficients of determination were (R^2) higher, the RMSE lower and the MEP values within acceptable error limits (±5 %) for these learning algorithms.
3. While the coefficients of determination for the main cutting force and feed force resulting from the regression analysis were 98 and 85 %, respectively, in the ANN model, the coefficients of determination of the cutting forces for both the training and the testing set were more than 99 %. In addition, when the results of the predictions made with both modelling techniques were considered, it was concluded that the error values obtained with ANNs were rather lower than the error values obtained with the regression analysis.
4. It was determined that the ANN results were within acceptable error limits (±5 %). Therefore, it is recommended that ANNs be used for the prediction of cutting forces instead of conducting experimental

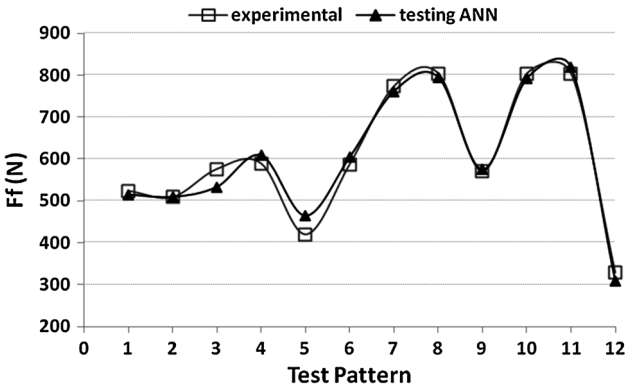

Fig. 10 Matching of the experimental and ANN values for testing sets of feed forces

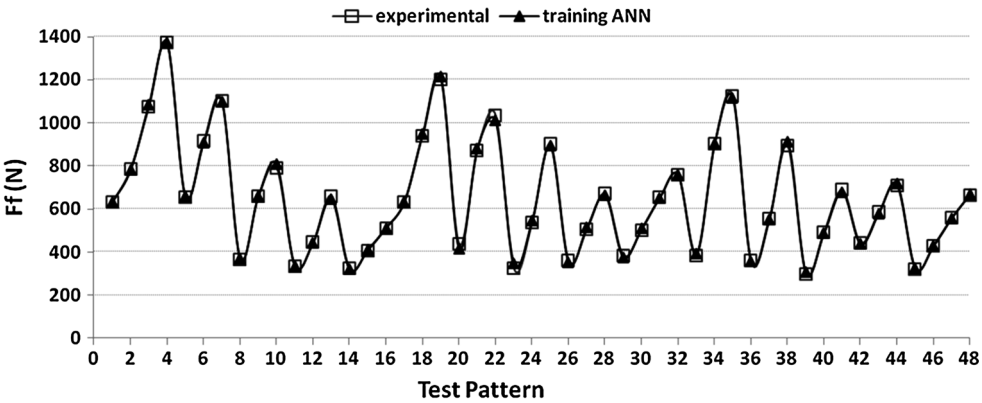

Fig. 11 Matching of the experimental and ANN values for training sets of feed forces

Table 9 Statistical values for the cutting forces

Cutting forces	Learning algorithm	Number of neurons	Training data			Testing data		
			RMSE	R^2	MEP	RMSE	R^2	MEP
F_c	SCG	7	0.006674	0.999830	1.396251	0.007364	0.999771	1.447662
F_f	LM	6	0.006333	0.999804	1.295207	0.013873	0.998816	3.235189

Table 10 Weight values between the input and hidden layers for main cutting force (F_c)

	$E_i = w_1 \times (C_t/4) + w_2 \times (V/300) + w_3 \times (f \times 3) + \theta_i$			
i	w_1	w_2	w_3	θ_i
1	−4.1909	2.9232	−9.8956	13.6210
2	−6.4122	−2.7505	2.2049	5.2403
3	−0.0913	11.3170	−3.3924	−3.9022
4	0.0837	8.6899	−6.2375	5.1409
5	0.9519	1.0918	4.4842	−4.3567
6	1.6732	2.4717	14.3907	−5.3042
7	8.8149	8.5404	0.7519	−2.9236

Table 11 Weight values between input and hidden layers for feed force (F_f)

	$E_i = w_1 \times (C_t/4) + w_2 \times (V/300) + w_3 \times (f \times 3) + \theta_i$			
i	w_1	w_2	w_3	θ_i
1	−1.0495	15.1393	−3.3832	−9.3499
2	32.1946	−404.0544	79.3005	28.5831
3	1.9708	6.1249	16.0888	−7.6747
4	0.6327	1.5751	−1.1181	−1.6247
5	6.9974	5.8535	−1.6233	2.6603
6	−75.4199	4.2948	8.0672	14.3671

Table 12 Maximum errors for cutting forces

Parameters	Max. error (%)	Coating type	Cutting speed (m/min)	Feed rate (mm/rev)
F_c (N)	3.394	TiN + Al_2O_3 + TiCN	100	0.1
F_f (N)	10.386	TiN + Al_2O_3 + TiCN	75	0.05

studies, which are complicated, expensive and time consuming.

5. ANNs have significant advantages when compared with other conventional modelling techniques in terms of speed, simplicity and learning capacity from samples. This study has shown that ANNs constitute a good alternative to conventional modelling techniques for the prediction of cutting forces.

References

1. Ciftci I (2005) The influence of cutting tool coating and cutting speed on cutting forces and surface roughness in machining of austenitic stainless steels. J Fac Eng Arch Gazi Univ 20(2):205–209
2. Ozer A, Bahceci E (2009) Machinability of AISI 410 martensitic stainless steels depending on cutting tool and coating. J Fac Eng Arch Gazi Univ 24(4):693–698
3. M'Saoubi R, Chandrasekaran H (2011) Experimental study and modeling of tool temperature distribution in orthogonal cutting of AISI 316L and AISI 3115 steels. Int J Adv Manuf Technol 56:865–877
4. Waled ME, Tahir IK (2011) Eutectic bonding of austenitic stainless steel 316L to magnesium alloy AZ31 using copper interlayer. Int J Adv Manuf Technol 55:235–241
5. Kıvak T, Samtas G, Çiçek A (2012) Taguchi method based optimisation of drilling parameters in drilling of AISI 316 steel with PVD monolayer and multilayer coated HSS drills. Measurement 45:1547–1557
6. Venkata Rao R, Kalyankar VD (2012) Parameter optimization of machining processes using a new optimization algorithm. Mater Manuf Process 27:978–985
7. Thomas TR (1982) Rough surface. Longman, New York
8. Aslantas K, Ucun I, Gok K (2008) Evaluation of the performance of CBN tools when turning austempered ductile iron material. J Manuf Sci Eng 130(5):54503–54507
9. Aslantas K, Ucun I (2009) The performance of ceramic and cermet cutting tools for the machining of austempered ductile iron. Int J Adv Manuf Technol 41:642–650
10. Aslantas K, Ucun I, Cicek A (2012) Tool life and wear mechanism of coated and uncoated Al_2O_3/TiCN mixed ceramic tools in turning hardened alloy steel. Wear 274–275:442–451
11. Trent EM (1984) Metal cutting, 2nd edn. Butterworths, London
12. Gunay M, Aslan E, Korkut I et al (2004) Investigation of the effect of rake angle on main cutting force. Int J Mach Tools Manuf 44:953–959
13. Fernández-Abia AI, Barreiro J, de Lacalle LNL et al (2011) Effect of very high cutting speeds on shearing, cutting forces and roughness in dry turning of austenitic stainless steels. Int J Adv Manuf Technol 57:61–71
14. Totis G, Sortino M (2011) Development of a modular dynamometer for triaxial cutting force measurement in turning. Int J Mach Tools Manuf 51:34–42
15. Kuram E, Cetin MH, Ozcelik B et al (2012) Performance analysis of developed vegetable-based cutting fluids by D-optimal experimental design in turning process. Int J Comput Integr Manuf 25(12):1165–1181
16. Ucun I, Eleren A, Aslantas K (2008) Prediction of cutting forces and surface roughness in turning of austempered ductile iron using fuzzy logic approach. Electron J Mach Technol 5(2):13–21
17. Korkut I, Acir A, Boy M (2011) Application of regression and artificial neural network analysis in modelling of tool-chip interface temperature in machining. Expert Syst Appl 38:11651–11656
18. Pal SK, Chakraborty D (2005) Surface roughness prediction in turning using artificial neural network. Neural Comput Appl 14:319–324
19. Venkatesan D, Kannan K, Saravanan R (2009) A genetic algorithm-based artificial neural network model for the optimization of machining processes. Neural Comput Appl 18:135–140
20. Koklu U (2013) Optimisation of machining parameters in interrupted cylindrical grinding using the Grey-based Taguchi method. Int J Comput Integr Manuf 26(8):696–702
21. Fang N, Srinivasa Pai P, Edwards N (2010) Prediction of built-up edge formation in machining with round edge and sharp tools using a neural network approach. Int J Comput Integr Manuf 23(11):1002–1014
22. Jha MN, Pratihar DK, Dey V et al (2011) Study on electron beam butt welding of austenitic stainless steel 304 plates and its input-output modelling using neural networks. Proc Inst Mech Eng Part B: J Eng Manuf 225:2051–2070
23. Silva JA, Abellan-Nebot JV, Siller HR et al (2013) Adaptive control optimisation system for minimising production cost in hard milling operations. Int J Comput Integr Manuf. doi:10.1080/0951192X.2012.749535

24. Anderson D, McNeill G (1992) Artificial neural networks technology. Kaman Sciences Corporation, New York
25. Haykin S (1994) Neural networks: a comprehensive foundation. Macmillan, New York
26. Hao W, Zhu X, Li X et al (2006) Prediction of cutting force for self-propelled rotary tool using artificial neural networks. J Mater Process Technol 180:23–29
27. Suksawat B (2010) Chip form classification and main cutting force prediction of cast nylon in turning operation using artificial neural network. Int Conf Control Autom Syst Gyeonggi-do, Korea, pp 172–175
28. Ozkan IA, Saritas I, Yaldiz S (2009) Prediction of cutting forces and tool tip temperature in turning using artificial neural network. IATS'09, Karabük, Turkey
29. Yilmaz S, Arici AA, Feyzullahoglu E (2011) Surface roughness prediction in machining of cast polyamide using neural network. Neural Comput Appl 20:1249–1254
30. Ucun I, Aslantas K (2011) Numerical simulation of orthogonal machining process using multilayer and single-layer coated tools. Int J Adv Manuf Technol 54:899–910
31. Efe MO, Kaynak O (2000) Artificial neural network and applications. Bogazici University Publishing, İstanbul
32. Sagiroglu S, Besdok E, Erler M (2003) Applications of Artificial intelligence in engineering: artificial neural network. Ufuk Book-Stationer, Kayseri
33. Gauri SK, Chakraborty S (2008) Improved recognition of control chart patterns using artificial neural networks. Int J Adv Manuf Technol 36:1191–1201
34. Rahimi-Ajdadi F, Abbaspour-Gilandeh Y (2011) Artificial neural network and stepwise multiple range regression methods for prediction of tractor fuel consumption. Meas 44:2104–2111
35. Kohli A, Dixit US (2005) A neural-network-based methodology for the prediction of surface roughness in a turning process. Int J Adv Manuf Technol 25:118–129
36. Pal SK, Chakraborty D (2005) Surface roughness prediction in turning using artificial neural network. Neural Comput Appl 14:319–324
37. Cus F, Zuperl U (2006) Approach to optimization of cutting conditions by using artificial neural networks. J Mater Process Technol 173:281–290
38. Al-Ahmari AMA (2007) Predictive machinability models for a selected hard material in turning operations. J Mater Process Technol 190:305–311
39. Davim JP, Gaitonde VN, Karnik SR (2008) Investigations into the effect of cutting conditions on surface roughness in turning of free machining steel by ANN models. J Mater Process Technol 205:16–23
40. Karnik SR, Gaitonde VN, Rubio JC et al (2008) Delamination analysis in high speed drilling of carbon fiber reinforced plastics (CFRP) using artificial neural network model. Mater Des 29:1768–1776
41. Chavoshi SZ, Tajdari M (2010) Surface roughness modelling in hard turning operation of AISI 4140 using CBN cutting tool. Int J Mater Form 3:233–239
42. Asilturk I, Tinkir M, El Monuayri H et al (2012) An intelligent system approach for surface roughness and vibrations prediction in cylindrical grinding. Int J Comput Integr Manuf 25(8):750–759
43. Bouacha K, Yallese MA, Mabrouki T, Rigal JF (2010) Statistical analysis of surface roughness and cutting forces using response surface methodology in hard turning of AISI 52100 bearing steel with CBN tool. Int J Refract Metals Hard Mater 28:349–361
44. Çiçek A, Kara F, Kivak T et al (2013) Evaluation of machinability of hardened and cryo-treated AISI H13 hot work tool steel with ceramic inserts. Int J Refract Metals Hard Mater 41:461–469
45. Yen YC, Jain A, Chigurupati P et al (2004) Computer simulation of orthogonal cutting using a tool with multiple coatings. Mach Sci Technol 8(2):305–326
46. Balaji AK, Mohan VS (2002) An effective cutting tool thermal conductivity based model for tool–chip contact in machining with multi-layer coated cutting tools. Mach Sci Technol 6(3):415–436
47. Rech J, Kusiak AJ, Battaglia L (2004) Tribological and thermal functions of cutting tool coatings. Surf Coat Technol 186(3): 364–371
48. Lalwani DI, Mehta NK, Jain PK (2008) Experimental investigations of cutting parameters influence on cutting forces and surface roughness in finish hard turning of MDN250 steel. J Mater Process Technol 206:167–179
49. Suresh R, Basavarajappa S, Gaitonde VN et al (2012) Machinability investigations on hardened AISI 4340 steel using coated carbide insert. Int J Refract Metals Hard Mater 33:75–86
50. Aurich JC, Eyrisch T, Zimmermann M (2012) Effect of the coating system on the tool performance when turning heat treated AISI 4140. Procedia CIRP 1:214–219